J Math Chem (2014) 52:2074–2086
DOI 10.1007/s10910-014-0367-4

ORIGINAL PAPER

Polarized gating assisted generation of the ultrashort extreme-ultraviolet sources

Liqiang Feng · Hang Liu · Xingjiang Liu

Received: 13 May 2014 / Accepted: 22 May 2014 / Published online: 31 May 2014

Abstract High-order harmonic emission and attosecond extreme-ultraviolet pulse generation have been theoretically investigated by controlling the two-color polarized laser field. The results show that when the polarized angle between the two pulses is arranged at $\theta = 0.2\,\pi$, not only the harmonic cutoff is extended, but also the modulation on the harmonic spectrum is decreased. Further, by optimizing the laser parameters, a supercontinuum with the 270 eV bandwidth can be obtained, which results in a series of isolated 38 as pulses. Finally, by investigating the pulse duration effect on the harmonic emission, we find that this two-color polarized gating scheme can also be achieved by the multi-cycle pulse region, which is much better for experimental realization.

Keywords High-order harmonic generation · Isolated pulse · Two-color polarized laser field

L. Feng (✉)
College of Science, Liaoning University of Technology, Jinzhou 121000, China
e-mail: lqfeng_lngy@126.com

L. Feng
State Key Laboratory of Molecular Reaction Dynamics, Dalian Institute of Chemical Physics, Chinese Academy of Sciences, Dalian 116023, China

H. Liu
School of Chemical and Environmental Engineering, Liaoning University of Technology, Jinzhou 121000, China

X. Liu
School of Materials Science and Engineering, Liaoning University of Technology, Jinzhou 121000, China

1 Introduction

Attosecond extreme-ultraviolet pulse (10^{-18} s) generation has been widely investigated due to its important applications in exploring and controlling the ultrafast dynamic processes in atoms and molecules [1–3]. Currently, there are several methods for the generation of the attosecond pulse, such as stimulated Raman scattering [4], relativistic nonlinear Thomson scattering [5], and high-order harmonic generation (HHG) [6]. Among them HHG as the most effective and the only method to experimentally generate isolated attosecond pulse has been intensively investigated during the last two decades [7–9].

Currently, the generation of the attosecond pulse (train) in HHG can be well explained by the semi-classical 'three-step' model by Corkum [10] or the quantum mechanical version by Lewenstein et al. [11]: where harmonics are emitted through the steps of tunneling ionization, acceleration and recombination. Usually, this process occurs at every half optical cycle of the laser field and there correspond two major electron paths for a given frequency of the emitted photon: the long quantum path (with earlier ionization and later recollision) and the short quantum path (with later ionization and earlier recollision) [12]. Each of them produces an attosecond pulse at every half-cycle, thus, an attosecond pulse train with four main bursts in an optical cycle is formed. However, for practical application, an isolated attosecond pulse is more useful as the attosecond-resolution probing and exploring tool. Therefore, how to select one of the quantum paths becomes an interesting and important issue. So far, there are several successful methods to achieve this goal, i.e. the few-cycle pulse [13], the two-color or multi-color mixing method [14–16], the terahertz or the static field controlling scheme [17], and the chirped pulse scheme [18] etc.

However, the synthesized fields used in the above schemes are almost the linear polarization (parallel). As we know that the HHG process is highly dependent on the ellipticity of the laser field, therefore, the time-varying polarization gating is a very important technique to the harmonic selection. For instance, recent investigations show that the synthesized field (two or three color) with the orthogonal polarization can also been used for the harmonic path selection and the attosecond pulse generation [19–23], i.e. Yu et al. [24] theoretically obtained a single 115 as pulse by using an orthogonal two-color laser field, consisting of a 9 fs/800 nm pulse in x direction and a 9 fs/1,300 nm pulse in y direction; Xia et al. [25] theoretically obtained an isolated 75 as pulse by using an orthogonal three-color laser field, consisting of a 12 fs/800 nm pulse in x direction and the combination of a 12.5 fs/2,000 nm pulse and a weak static field in y direction etc. However, only few literatures [26,27] have been reported on the investigation of the polarized angle of the synthesized laser field.

Thus, in this paper, by controlling the polarized two-color field, we further investigate harmonic emission and the attosecond pulse generation. It shows that with the introduction of the polarized angle at $\theta = 0.2\,\pi$, an ultrabroad 270 eV bandwidth with the dominant short quantum path contribution has been obtained, which can support a series of isolated 38 as pulses.

2 Theory and method

In our numerical calculations, the HHG spectra can be investigated by solving the time-dependent Schrödinger equation (TDSE). In the dipole approximation and the length gauge, the TDSE is given by [atomic units (a.u.) are used throughout this paper unless stated otherwise],

$$i\frac{\partial\varphi(x,y,t)}{\partial t}=\left[-\frac{1}{2}\frac{\partial^2}{\partial x^2}-\frac{1}{2}\frac{\partial^2}{\partial y^2}+V(x,y)+xE_x(t)+yE_y(t)\right]\varphi(x,y,t), \quad (1)$$

where $V(x,y)=-1.0/\sqrt{x^2+y^2+a}$ is the soft Coulomb potential with a = 0.07 to match the ionization potential of 24.6 eV for the ground state of He. x and y are the two-dimensional (2D) electronic coordinates, which are defined by -250 a.u. $<$ x, y $<$ 250 a.u. with $\Delta x=\Delta y=0.5$ a.u.. The absorbing regions on x and y extend over the last 100 grid points. The time space is chosen to be Δt = 0.1 a.u.. The length of time t for the time evolution is 10 T, where T is the optical cycle of the 800 nm pulse. Propagation of the time-dependent electronic wave function $\varphi(x,\ y,\ t)$ can be carried out using the standard second-order split-operator method [28–30]. The synthesized laser field is expressed as,

$$\begin{aligned}\vec{E}(t)=&\left[E_1 f_1(t)\cos(\omega_1 t+\varphi_1)+E_2 f_2(t)\cos(\theta)\cos(\omega_2 t+\varphi_2)\right]\widehat{x}\\&+E_2 f_2(t)\sin(\theta)\cos(\omega_2 t+\varphi_2)\hat{y}\end{aligned} \quad (2)$$

Here E_i, ω_i and φ_i (i = 1, 2) are the amplitudes, the frequencies and the relative angles of the 5 fs/800 nm fundamental pulse and 10 fs/1,200 nm controlling pulses. θ is the polarized angle between the two pulses (the angle between the two polarization axes). The envelope function is,

$$f_i(t)=\exp[-4\ln(2)t^2/\tau_i^2], \quad (3)$$

where τ_i (i = 1, 2) are the corresponding pulse durations of the two pulses.

According to the Ehrenfest theorem [31], the time-dependent dipole acceleration can be written in the form,

$$\begin{aligned}a(t)&=-\langle\varphi(x,y,t)|\nabla\overrightarrow{V}(x,y)+\vec{E}(t)\,|\varphi(x,y,t)\rangle\\&=-\langle\varphi(x,y,t)|\left(\frac{\partial V(x,y)}{\partial x}+E_x(t)\right)\overrightarrow{e}_x+\left(\frac{\partial V(x,y)}{\partial y}+E_y(t)\right)\vec{e}_y\,|\varphi(x,y,t)\rangle\\&=a_x(t)\overrightarrow{e}_x+a_y(t)\vec{e}_y\end{aligned} \quad (4)$$

The HHG spectrum can be obtained by Fourier transforming the time-dependent dipole acceleration a(t) [32–34],

$$S(\omega_1)\sim\left|\int\exp(-i\omega_1 t)a(t)dt\right|^2$$

$$= \left| \int \exp(-i\omega_1 t)(a_x(t)\vec{e}_x + a_y(t)\vec{e}_y)dt \right|^2$$
$$\sim S_x(\omega_1) + S_y(\omega_1) \quad (5)$$

Finally, the attosecond pulse can be obtained by harmonic superposing as follows,

$$I(t) = \left| \sum_q a_q e^{iq\omega_1 t} \right|^2, \quad (6)$$

where $a_q = \int a(t)e^{-iq\omega_1 t}dt$.

3 Results and discussion

Figure 1a shows the HHG spectra from the single-color 800 and 1,200 nm pulses cases. The laser parameters are chosen to be 5 fs/800 nm, $I_1 = 1.0\times10^{15}$ W/cm^2, $\varphi_1 = 0.0\,\pi$ and 10 fs/1,200 nm, $I_2 = 1.0 \times 10^{14}$ W/cm^2, $\varphi_2 = 0.0\,\pi$, respectively. It shows that the harmonic cutoff energies are respective the $138\omega_1$ for single 800 nm pulse and the $65\omega_2$ for single 1,200 nm pulse, which is in quantitative agreement with the famous cutoff energy rule $I_p + 3.17U_p$ (I_p is the ionization energy and $U_p = E_i^2/4\omega_i^2$ (i = 1, 2) is the ponderomotive energy of the free electron). Figure 1b shows the HHG spectra driven by the above two-color polarized pulse. Clearly, for the linearly polarized two-color field case ($\theta = 0.0\,\pi$), the harmonic has been remarkably extended to the $267\omega_1$ in comparison with the single-color two cases (Fig. 1b solid black line). However, the modulation on the harmonic spectrum is too large to support an isolated attosecond pulse. With the increasing of the polarized angle θ, we see that the harmonic cutoffs and the harmonic yields are both decreased (see Fig. 1c the original intensities of the harmonic spectra), which is unbeneficial to the pulse generation, but the harmonic plateaus become smooth, which is beneficial to the isolated pulse selection. Thus, through our calculations, $\theta \in [0.0\pi, 0.5\pi]$ is much better for attosecond pulse generation, especially for the $\theta = 0.2\,\pi$ case (Fig. 1b solid red line), a 166 eV bandwidth with a proper intensity can be obtained.

Figure 2a, d show the HHG spectra in x and y components for the cases of the above two-color polarized pulses with $\theta = 0.2\,\pi$ and $0.5\,\pi$, respectively. As we see, the HHG have contributions in both x and y components, thus, the ellipticity will be generated in the harmonic emission process. According to Zhou et al.'s [35] investigation, we know that the ellipticity of the harmonic emission can be defined as $\xi = \sqrt{I_{minor}/I_{major}}$, where I_{minor} and I_{major} are the intensity of the minor and major axis of the HHG and the corresponding results are shown in Fig. 2b, e. Clearly, the harmonic emission from the two-color polarized gating pulse can be strongly elliptically polarized, especially for the low harmonic orders. However, for the high harmonic orders, especially for the plateau region, the especially of the harmonic almost equals to a fixed value, moreover, with the increasing of the polarized angle θ, this fixed value will also be enhanced (i.e. $\varepsilon \approx 0.15$ for the $\theta = 0.2\,\pi$ case and $\varepsilon \approx 0.4$ for the $\theta = 0.5\,\pi$ case, as shown in Fig. 2c, f).

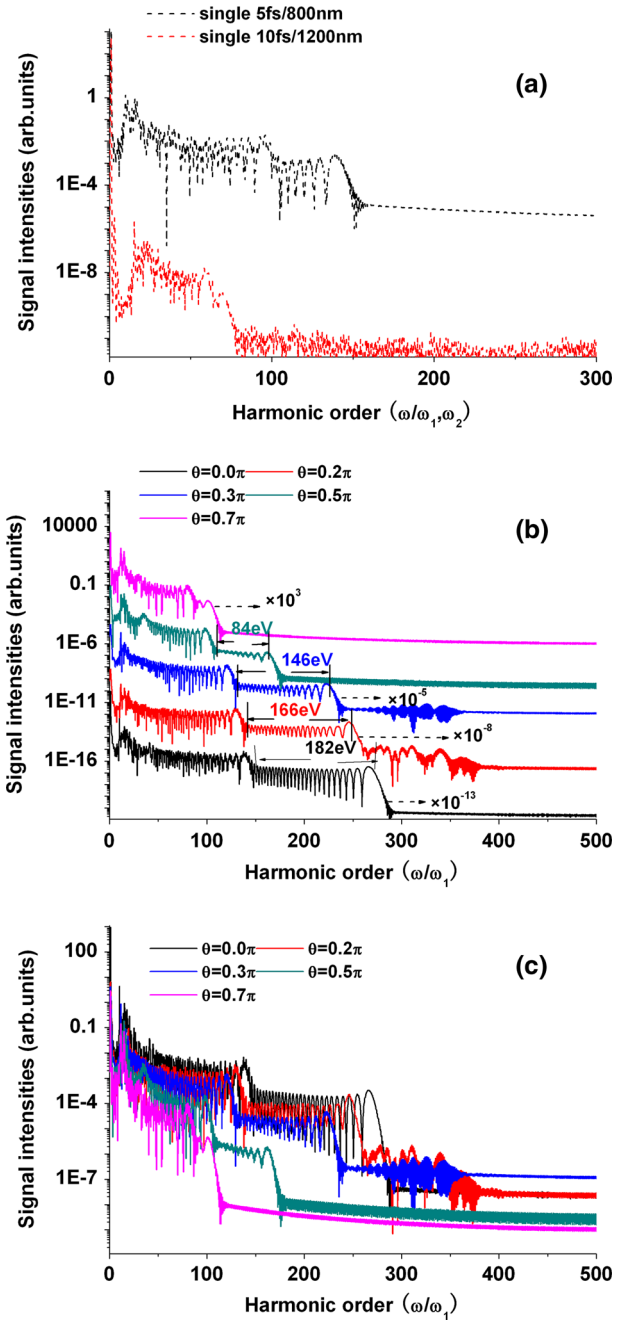

Fig. 1 **a** HHG spectra of the single 5 fs/800 nm pulse (*dash black line*) and single 10 fs/1,200 nm (*dash red line*). **b** HHG spectra of the two-color polarized pulse with $\theta = 0.0\,\pi$ (*solid black line*), $0.2\,\pi$ (*solid red line*), $0.3\,\pi$ (*solid blue line*), $0.5\,\pi$ (*solid dark cyan line*) and $0.7\,\pi$ (*solid magenta line*). To better identify, each of the harmonic has been multiply by a coefficient. **c** HHG spectra as similar as those in **b** but with the original yields (Color figure online)

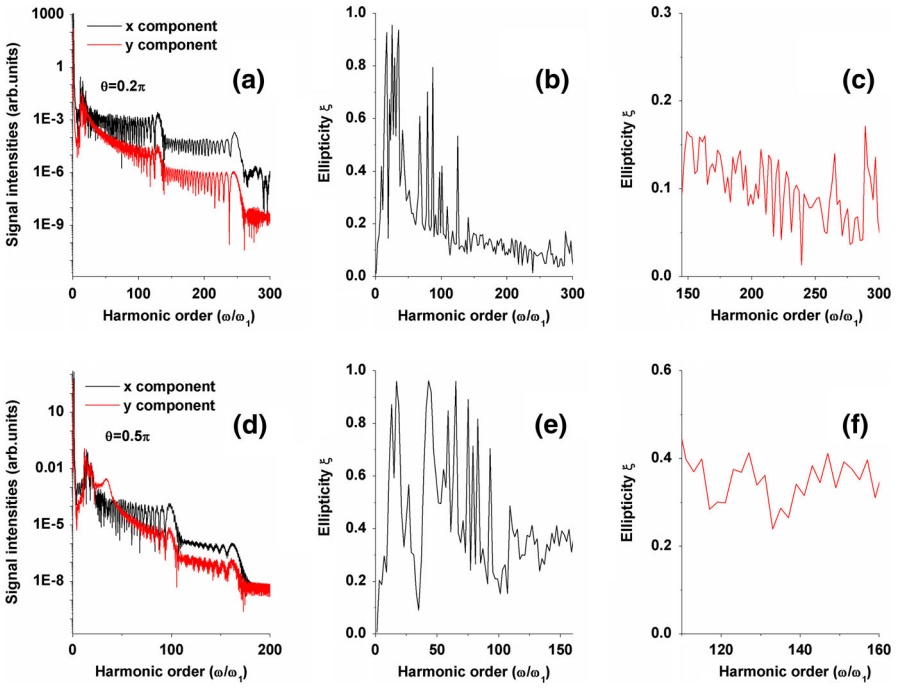

Fig. 2 **a**, **d** HHG spectra in x and y components for the cases of the two-color polarized pulses with $\theta = 0.2\,\pi$ and $0.5\,\pi$, respectively. **b**, **e** Ellipticity ε of the harmonic emission for the cases of the $\theta = 0.2\,\pi$ and $0.5\,\pi$, respectively. **c**, **f** The high graphics of **b** and **e** (Color figure online)

To better understand the harmonic emission process, in Fig. 3, we present the time-frequency distributions of HHG spectra, obtained by using the wavelet transformation of the dipole acceleration a(t) [36],

$$A(t, \omega_1) = \int a(t')\sqrt{\omega_1} W(\omega_1(t' - t))dt', \tag{7}$$

where $W(\omega_1(t' - t))$ is the Morlet wavelet with the formula of,

$$W(\xi) = \left(\frac{1}{\sqrt{\alpha}}\right) e^{i\xi} e^{-\xi^2/2\alpha^2}, \tag{8}$$

here $\alpha = 30$ in our calculations. For the single-color two cases, as shown in Fig. 3b, c, there are three main emission bursts on the harmonic emission process, and the maximum harmonic cutoff is agreement well with the quantum result shown in Fig. 1. Moreover, each burst receives similar contributions from the long quantum path (right path) having earlier ionization and later recollision and the short quantum path (left path) with later ionization but earlier recollision, which is responsible for the large interference on the harmonics [12,37]. For the linearly-polarized two-color case ($\theta = \varphi_1 = \varphi_2 = 0.0\,\pi$), as shown in Fig. 3d, we see that the maximum emission burst is remarkably enhanced compared with the single-color two cases. According to the

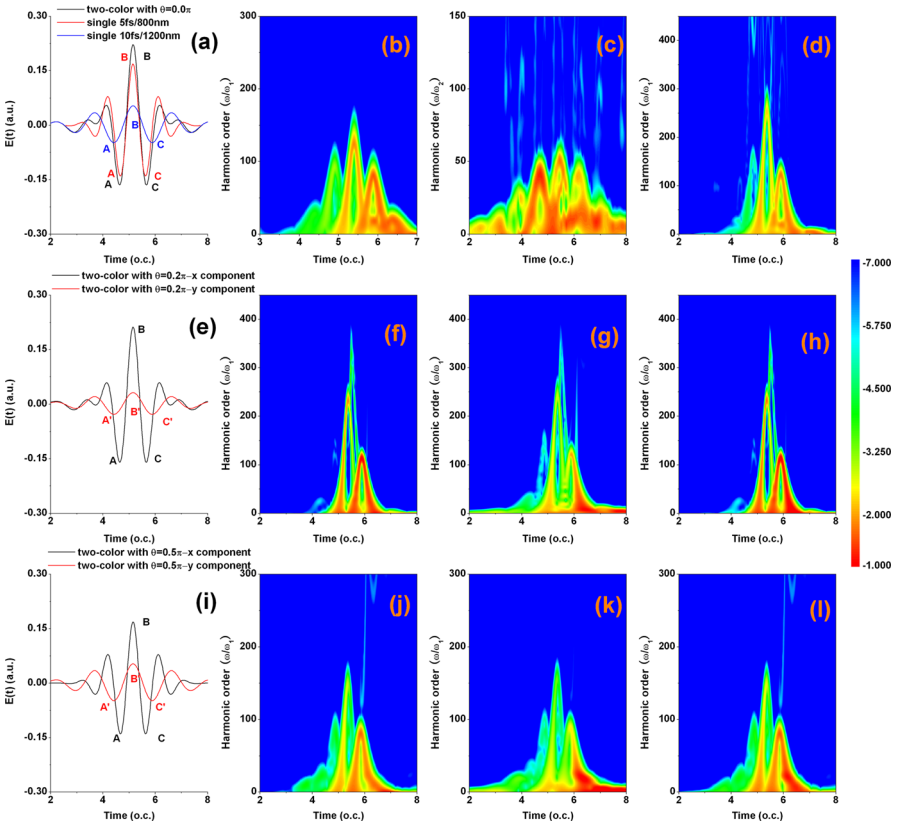

Fig. 3 **a** The profiles of the single 5 fs/800 nm pulse, 10 fs/1,200 nm and the two-color polarized pulse with $\theta = 0.0\,\pi$. **b–d** The time-frequency harmonic distributions for the above three cases. **e** The profiles of the two-color polarized pulse with $\theta = 0.2\,\pi$ in x and y components. **f–h** The time-frequency harmonic distributions of the $\theta = 0.2\,\pi$ case for the x, y components and the total harmonic spectrum, respectively. **i–l** The similar results as those in **e–h** but for the case of $\theta = 0.5\,\pi$. o.c. means the optical cycle of 800 nm pulse in all the following figures unless stated otherwise

'three-step' model, the harmonic emission is caused by the ionization–acceleration–recombination, and each harmonic emission burst/cutoff is determined by the half-cycle profile. In the present laser fields, the maximum harmonic emission burst is determined by the A–B–C processes of the laser fields, as shown in Fig. 3a. Clearly, due to the enhancing of the pulse intensity, the A–B–C process of the linearly-polarized two-color case has been enhanced, thus, the electron gained much more energy and spent a little more time in accelerating and returning processes, which is responsible for the extension of the harmonic cutoff. While with the introduction of the polarized angle, as shown in Fig. 3e and i for the cases of $\theta = 0.2\,\pi$ and $0.5\,\pi$, we see that due to the varieties of the laser fields, both the A–B–C and the A'–B'–C' processes in the x and y components of the synthesized laser field are weaker than that in the linearly-polarized two-color case ($\theta = 0.0\,\pi$), thus, resulting in the suppressing of the maximum harmonic emission bursts in x, y components and the total harmonic,

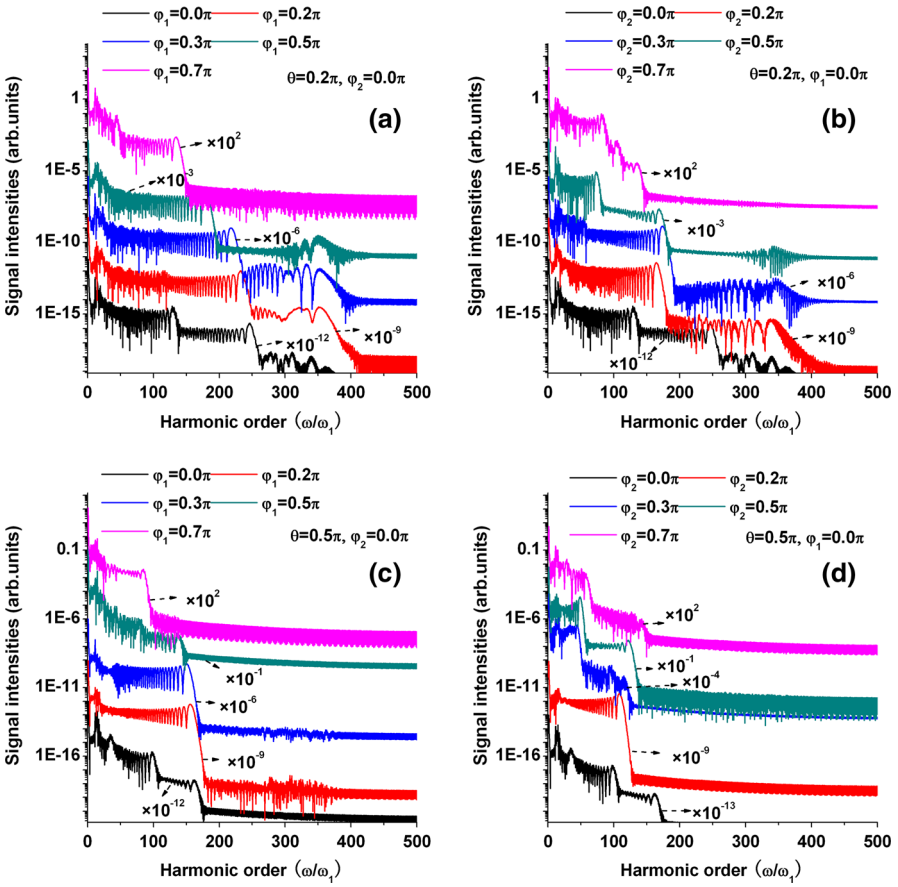

Fig. 4 **a**, **b** HHG spectra as a function of the harmonic order and the relative angles φ_1 and φ_2, respectively. The polarized angle of the two pulse is chosen to be $\theta = 0.2\,\pi$. **c**, **d** The similar results as those in **a**, **b** but for the case of $\theta = 0.5\,\pi$

as shown in Fig. 3f–h (for $\theta = 0.2\,\pi$ case) and j–l (for $\theta = 0.5\,\pi$ case). Moreover, we see that with the increasing of the polarized angle, the amplitude of the dominant A–B–C process has been further suppressed, which is the main reason behind the harmonic decreased with the increasing of the polarized angle. Furthermore, due to the pulse is assigned in both x and y components, part of the quantum path trajectories have been counteracted, thus leading to the short quantum path is partially selected for the harmonic emission process, as shown in Fig. 3h, l, which is responsible for small modulation on the harmonic spectra in Fig. 1b.

Figure 4a–d show the relative angles (φ_1, φ_2) effects on the harmonic emission. The polarized angles of the two pulses are chosen to be $\theta = 0.2\,\pi$ (for Fig. 4a, b) and $\theta = 0.5\,\pi$ (for Fig. 4c, d), respectively. Clearly, we see that the maximum cutoff energy is achieved when relative angles $\varphi_1 = \varphi_2 = 0.0\,\pi$. Respective increasing of the relative angles φ_1 or φ_2, only leads to harmonic cutoffs move towards the low harmonic orders.

Figure 5a show the controlling wavelength effect on the harmonic emission. The other parameters are the same as those in Fig. 1b solid red line ($\theta = 0.2\,\pi,\ \varphi_1 = \varphi_2 = 0.0\,\pi$ case). As we know that the maximum harmonic cutoffs ($E_{max} = I_p + nU_p$) are decided by either the amplitude intensities (relating to the pulse intensities) or the widths (relating to the frequencies) of the half-cycle laser profiles. Thus, with the increasing of the controlling wavelength, the harmonic cutoff has been further extended due to the instantaneous reduction of the central frequency of the laser field, however, the large modulation on the harmonic plateau is unbeneficial to the attosecond pulse generation. Thus, through our calculations, $\lambda_2 = 1{,}200$ nm is the suitable controlling wavelength for harmonic selection. Figure 5b shows the controlling pulse intensity effect on the harmonic extension. Clearly, from the above analyses, we know that with the increasing of the controlling pulse intensity, the harmonic cutoff can be enhanced, which means the higher pulse intensity we chose, the broader plateau we will get. However, the long wavelength controlling pulse with the higher intensity is still not easier to obtain in experiment. Thus, in this paper, we choose $I_2 = 3.0\times10^{14}$ W/cm^2 as a proper controlling pulse intensity and a supercontinuum with the 270 eV bandwidth can be obtained, which will favorite to support the isolated attosecond pulse. Figure 5c shows the pulse duration effect on the harmonic generation. Clearly, with the variety of τ_2, the harmonic spectra produce almost no change (at least for $\tau_2 = 20$ fs). While with the increasing of τ_1, the 2nd maximum harmonic cutoff is a little enhanced, resulting in the reducing of the harmonic plateau, but it can also be accepted for the isolated pulse generation (for $\tau_1 = 10$ fs). Therefore, based on the practical application, choosing the longer pulse durations ($\tau_1 = 10$ fs and $\tau_2 = 20$ fs) is much better for experimental realization.

Figure 6 shows the temporal profiles of the attosecond pulses. In particular, by respectively superposing the harmonics of the above few-cycle optimal synthesized field case (Fig. 5b solid blue line) from the 190th to the 240th orders (photon energies between 294 and 372 eV), from the 240th to the 290th orders (photon energies between 372 and 449 eV) and from the 290th to the 340th orders (photon energies between 449 and 527 eV), three isolated extreme-ultraviolet pulses with durations of 38 as can be obtained, as shown in Fig. 6a. Further, if we choose the harmonic spectrum of the multi-cycle synthesized field (Fig. 5c solid green line 10 fs + 20 fs) and by properly superposing the harmonics from the 220th to the 270th orders (photon energies between 341 and 418 eV) and from the 270th to the 320th orders (photon energies between 418 and 496 eV), another two isolated 38 as pulses can also be obtained, as shown in Fig. 6b. To illuminate the conversion efficiency and the advantages for using the present two-color polarized gating pulse, we also present the attosecond pulse generation from the no gating and the other gating-schemes. For instance, (1) by superposing the harmonics of linearly-polarized two-color case (no gating case) from the 150th to the 190th orders and from the 190th to the 230th orders, two attosecond pulse trains with durations of 40as can be obtained, as shown in Fig. 6c. (2) By superposing the harmonics of two-color polarized pulse with $\theta = 0.5\,\pi$ case from the 110th to the 150th orders, an isolated 60 as pulse can be obtained, as shown in Fig. 6d. However, the generated pulse intensity is one order of magnitude lower than that in the optimal two-color polarized case. (3) By superposing the harmonics of two-color polarized pulse with $\theta = 0.2\,\pi$ and $\lambda_2 = 800$ nm case from the 160th to the 200th orders, an

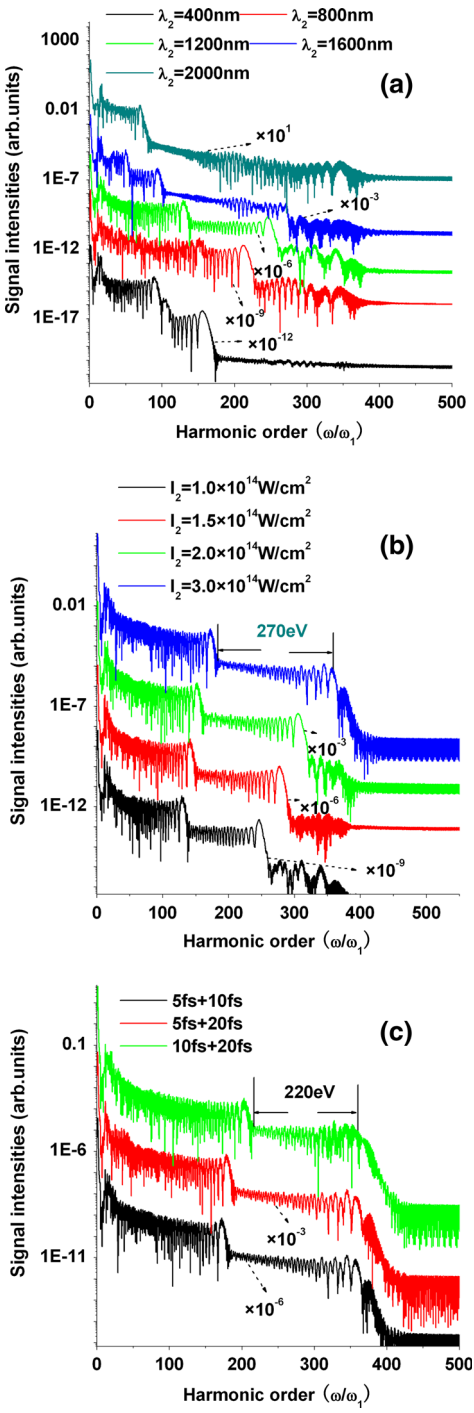

Fig. 5 **a** Controlling pulse wavelength effect on the harmonic emission. **b** Controlling pulse intensity effect on the harmonic extension. **c** Pulse duration effect on the harmonic generation. The other parameters are the same as those in Fig. 1a *solid red line* (Color figure online)

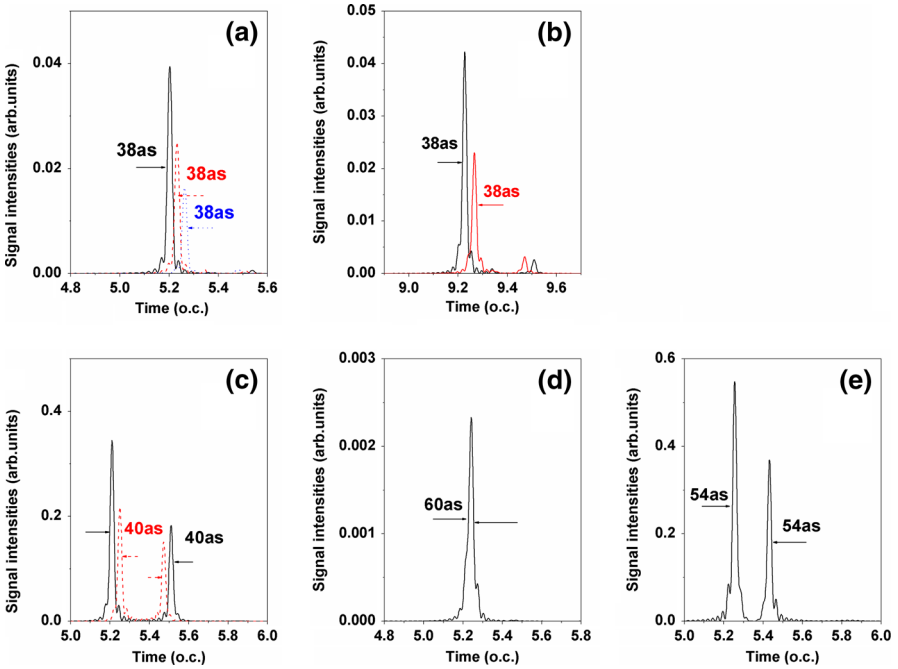

Fig. 6 **a** The temporal profiles of the attosecond pulses by superposing harmonics of (**a**) the optimal few-cycle synthesized field case from the 190th to the 240th orders, from the 240th to the 290th orders and from the 290th to the 340th orders; **b** the multi-cycle synthesized field case from the 220th to the 270th orders and from the 270th to the 320th orders; **c** the linearly polarized two-color field case ($\theta = 0.0\,\pi$) from the 150th to the 190th orders and from the 190th to the 230th orders; **d** the two-color polarized field with $\theta = 0.5\,\pi$ case from the 110th to the 150th orders; **e** the two-color polarized field with $\theta = 0.2\,\pi$ and $\lambda_2 = 800\,\text{nm}$ case from the 160th to the 200th orders (Color figure online)

attosecond pulse train as short as 54 as can be produced, as shown in Fig. 6e. Clearly, from a practical viewpoint, an isolated attosecond pulse with higher pulse intensity is especially in favor of the filed of the time-resolved dynamics measurement. Therefore, the present two-color polarized gating scheme (5 fs/800 nm + 10 fs/1,200 nm with $\theta = 0.2\,\pi$) is more favorable for the generation of the isolated attosecond sources. Moreover, the generated isolated 38as pulses with photon energies between 294 and 527 eV (wavelengths region between 2.3 and 4.2 nm) may bring useful insight into 3D biological imaging, nanolithography, XUV interferometry, exploring the atomic and molecular structure, etc.

4 Conclusion

In conclusion, we have theoretically investigated the generation of the harmonics and the attosecond extreme-ultraviolet pulses in the presence of the two-color polarized gating pulse. The results show that by properly choosing the polarized angle at $\theta = 0.2\,\pi$, not only the harmonic cutoff has been remarkably enhanced, resulting in a 270 eV bandwidth, but also the single short quantum path has been selected to con-

tribute to the harmonic emission. As a result, a series of isolated extreme-ultraviolet pulses with durations of 38 as can be obtained. Moreover, we also find that this polarized gating two-color scheme can also be realized in the multi-cycle pulse region, which is much better for experimental realization. Therefore, it is expected that our proposed scheme may bring useful insight into practical generation and application of the intense ultrashort attosecond extreme-ultraviolet pulses.

Acknowledgments This work was supported by the scientific research fund of Liaoning University of Technology, China (Nos. X201319 and X201312) and the scientific research fund of Liaoning provincial education department (No. L2012223).

References

1. P. Agostini, L. DiMauro, Rep. Prog. Phys. **67**, 813 (2004)
2. F. Krausz, M. Ivanov, Rev. Mod. Phys. **81**, 163 (2009)
3. W.L. Li, K.L. Han, J. Math. Chem. **51**, 1293 (2013)
4. A.E. Kaplan, Phys. Rev. Lett. **73**, 1243 (1994)
5. J. Gao, Phys. Rev. Lett. **93**, 243001 (2004)
6. L.Q. Feng, T.S. Chu, J. Chem. Phys. **136**, 054102 (2012)
7. T. Popmintchev, M.C. Chen, D. Popmintchev, P. Arpin et al., Science **336**, 1287 (2012)
8. E.J. Takahashi, T. Kanai, K.L. Ishikawa, Y. Nabekawa, K. Midorikawa, Phys. Rev. Lett. **101**, 253901 (2008)
9. K. Zhao, Q. Zhang, M. Chini, Y. Wu, X.W. Wang, Z.H. Chang, Opt. Lett. **37**, 3891 (2012)
10. P.B. Corkum, Phys. Rev. Lett. **71**, 1994 (1993)
11. M. Lewenstein, P. Balcou, M.Y. Ivanov, A. L'Huillier, P.B. Corkum, Phys. Rev. A **49**, 2117 (1994)
12. Y. Mairesse, A.D. Bohan, L.J. Frasinski, H. Merdji, L.C. Dinu, P. Monchicourt, P. Breger, M. Kovačev, R. Taïeb, B. Carré, H.G. Muller, P. Agostini, P. Salières, Science **302**, 1540 (2003)
13. E. Goulielmakis, M. Schultze, M. Hofstetter, V.S. Yakovlev, J. Gagnon, M. Uiberacker, A.L. Aquila, E.M. Gullikson, D.T. Attwood, R. Kienberger, F. Krausz, U. Kleineberg, Science **320**, 1614 (2008)
14. Z. Zeng, Y. Cheng, X. Song, R. Li, Z. Xu, Phys. Rev. Lett. **98**, 203901 (2007)
15. P.F. Lan, P.X. Lu, W. Cao, Y.H. Li, X.L. Wang, Phys. Rev. A **76**, 011402 (2007)
16. L.Q. Feng, Y.B. Duan, T.S. Chu, Ann. Phys. (Berlin) **525**, 915 (2013)
17. G.J. Zhao, X.L. Guo, T.J. Shao, K. Xue, New J. Phys. **13**, 093035 (2011)
18. L.Q. Feng, T.S. Chu, Phys. Rev. A **84**, 053853 (2011)
19. Y. Xiang, J. Miao, Y.P. Niu, S.Q. Gong, R.X. Li, Z.Z. Xu, J. Phys. B At. Mol. Opt. Phys. **45**, 115601 (2012)
20. C.D. Liu, Z.N. Zeng, Y.H. Zheng, P. Liu, R.X. Li, Z.Z. Xu, Phys. Rev. A **85**, 043420 (2012)
21. Y.L. Yu, J.J. Xu, Y.X. Fu, H. Xiong, H. Xu, J.P. Yao, B. Zeng, W. Chu, J. Chen, Y. Cheng, Z.Z. Xu, Phys. Rev. A **80**, 053423 (2009)
22. M. Kitzler, X. Xie, A. Scrinzi, A. Baltuska, Phys. Rev. A **76**, 011801 (2007)
23. J.J. Xu, Phys. Rev. A **83**, 033823 (2011)
24. Y.L. Yu, X.H. Song, Y.X. Fu, R.X. Li, Y. Cheng, Z.Z. Xu, Opt. Express **16**, 686 (2008)
25. C.L. Xia, G.T. Zhang, J. Wu, X.S. Liu, Phys. Rev. A **81**, 043420 (2010)
26. W.Y. Hong, P.X. Lu, P.F. Lan, Q.G. Li, Q.B. Zhang, Z.Y. Yang, X.B. Wang, Phys. Rev. A **78**, 063407 (2008)
27. J.P. Yao, Y. Li, B. Zeng, H. Xiong, H. Xu, Y.X. Fu, W. Chu, J.L. Ni, X.J. Liu, J. Chen, Y. Cheng, Z.Z. Xu, Phys. Rev. A **82**, 023826 (2010)
28. J. Hu, K.L. Han, G.Z. He, Phys. Rev. Lett. **95**, 123001 (2005)
29. T.S. Chu, Y. Zhang, K.L. Han, Int. Rev. Phys. Chem. **25**, 201 (2006)
30. J.A. Fleck Jr, J.R. Morris, M.D. Feit, Appl. Phys. **10**, 129 (1976)
31. K. Burnett, V.C. Reed, J. Cooper, P.L. Knight, Phys. Rev. A **45**, 3347 (1992)
32. R.F. Lu, H.X. He, Y.H. Guo, K.L. Han, J. Phys. B At. Mol. Opt. Phys. **42**, 225601 (2009)
33. L.Q. Feng, T.S. Chu, Commun. Comput. Chem. **1**, 52 (2013)
34. L.Q. Feng, T.S. Chu, Phys. Lett. A **375**, 3641 (2011)

35. X.B. Zhou, R. Lock, N. Wagner, W. Li, H.C. Kapteyn, M.M. Murnane, Phys. Rev. Lett. **102**, 073902 (2009)
36. J.J. Carrera, X.M. Tong, S.I. Chu, Phys. Rev. A **74**, 023404 (2006)
37. L.Q. Feng, T.S. Chu, IEEE J. Quantum Electron **48**, 1462 (2012)